

A statistical study of the post-impulsive-phase acceleration of flare-associated coronal mass ejections

X. Cheng¹, J. Zhang^{2,1}, M. D. Ding¹, and W. Poomvises²

Received _____; accepted _____

¹Department of Astronomy, Nanjing University, Nanjing, 210093, China;
dmd@nju.edu.cn

²Department of Computational and Data Sciences, George Mason University, 4400 University Drive, MSN 6A2, Fairfax, VA 22030

ABSTRACT

It is now generally accepted that the impulsive acceleration of a coronal mass ejection (CME) in the inner corona is closely correlated in time with the main energy release of the associated solar flare. In this paper, we examine in detail the post-impulsive-phase acceleration of a CME in the outer corona, which is the phase of evolution immediately following the main impulsive acceleration of the CME; this phase is believed to correspond to the decay phase of the associated flare. This observational study is based on a statistical sample of 247 CMEs that are associated with M- and X-class GOES soft X-ray flares from 1996 to 2006. We find that, from many examples of events, the CMEs associated with flares with long-decay time (or so-called long-duration flares) tend to have positive post-impulsive-phase acceleration, even though some of them have already obtained a high speed at the end of the impulsive acceleration but do not show a deceleration expected from the aerodynamic dragging of the background solar wind. On the other hand, the CMEs associated with flares of short-decay time tend to have significant deceleration. In the scattering plot of all events, there is a weak correlation between CME post-impulsive-phase acceleration and flare decay time. The CMEs deviated from the general trend are mostly slow or weak ones associated with flares of short-decay time; the deviation is caused by the relatively stronger solar wind dragging force for these events. The implications of our results on CME dynamics and CME-flare relations are discussed.

Subject headings: Sun: corona — Sun: coronal mass ejections (CMEs) — Sun: flares

1. Introduction

Coronal mass ejections (CMEs) are large-scale solar activities, which can release a vast amount of plasma and magnetic flux into the outer space and cause interplanetary disturbances and geomagnetic storms near the Earth (Gosling et al. 1993; Webb et al. 1994). Flares are viewed as strong energy release in the lower atmosphere of the Sun, where CMEs originate from but then depart from the Sun. The physical relationship between CMEs and flares has been a long-standing elusive issue in solar physics (Kahler 1992; Gosling et al. 1993; Hundhausen et al. 1999). Nevertheless, recent studies demonstrate that there is a strong physical connection between CMEs and flares. Zhang et al. (2001, 2004) studied the whole kinematic process of CMEs and found that those CMEs associated with flares usually undergo three distinct phases of evolution: the initiation phase, impulsive acceleration phase (mainly in the inner corona, $\leq 3.0 R_{\odot}$), and propagation phase (mostly in the outer corona). Furthermore, it was found that the three kinematic phases of CMEs coincide in time very well with the three phases of the associated flares: the pre-flare phase, flare main energy release phase or rise phase in soft X-ray, and flare decay phase, respectively (Zhang et al. 2001; Burkepile et al. 2004; Vrřnak et al. 2005). Recently, Temmer et al. (2008) analyzed the kinematics of two fast halo CMEs in the inner corona and found that there was a close connection between the acceleration profiles of the CMEs and the HXR light curves of the related flares. The almost synchronized temporal correlation between CME acceleration and flare flux increase indicates that both are driven by the same energy release process in the corona, especially within the impulsive phase. In other words, the dynamic evolution of these two phenomena may be different manifestation of the same energetic process, presumably via magnetic reconnection (Lin et al. 2000; Priest et al. 2002; Vrřnak et al. 2004; Zhang et al. 2006; Marićić et al. 2007; Temmer et al. 2008). Therefore, there is no apparent cause-effect relation between them, i.e., they do not cause one another.

In statistical views, the more intensive the flares are, the greater the possibility of the flares being associated with CMEs is (Andrews 2003; Yashiro et al. 2005). Yashiro et al. (2006) studied the power-law indices of the frequency distribution of flares, and found that flares with CMEs have a harder index of distribution than that of flares without CMEs. Zhang et al. (2003) found that flares associated with fast CMEs show clear footpoint-separating and two-ribbon brightening, while this feature is less often in flares associated with slow CMEs or without CMEs. MacQueen and Fisher (1983) and recently by St. Cyr et al. (1999) found that CMEs associated with flares or active regions have relatively higher speeds and tend to propagate with a constant speed or a negative acceleration in the outer corona; while ones associated with eruptive filaments have an initial slow speed and a positive acceleration in the outer corona. Using the latest CDAW CME catalog¹, Moon et al. (2002) also found similar results.

Nevertheless, the detailed relationship between the CME evolution following the impulsive acceleration phase and the properties of the flare decay phase has not been studied. Prior to LASCO, CMEs were commonly thought to propagate with nearly constant speed. Now we know that CMEs usually have a small acceleration or deceleration in the outer corona (about between 3.0 and 30.0 R_{\odot}) after they have been strongly accelerated in the inner corona (Andrews et al. 2001; Neupert et al. 2001; Zhang et al. 2001; Gallagher et al. 2003; Shanmugaraju et al. 2003). But, how this late evolution, dubbed as “post-impulsive-phase acceleration”, is related with flare characteristics is not clear, and therefore a detailed study on this issue is desirable. To quantify such evolution of CMEs, we introduce a fixed time window of two hours beginning at the peak time of the associated flare to calculate the acceleration (details of methods given in the next section). It is noted that the post-impulsive-phase acceleration is likely related to the residual acceleration

¹http://cdaw.gsfc.nasa.gov/CME_list

originally proposed by Chen et al. (2003). Based on their theoretical flux-rope model, Chen et al. (2003) specified the residual acceleration (in differ from the main acceleration) to the acceleration of the period that Lorentz self-force is decreased and the dragging force of solar wind starts to dominate. In the observational context, the residual acceleration was used by Zhang et al. (2006) in a more general sense to refer to the observed velocity change of CMEs following the impulsive acceleration phase, which can be practically separated by the peak time of the associated soft X-ray flares. In this paper, we investigate the post-impulsive-phase acceleration through both a case study of a variety of typical events and a statistical study as well. The main finding is that CMEs associated with long-decay flares tend to have positive post-impulsive-phase acceleration, and thus are more likely to reach a higher peak speed. In §2, we present the observations. Example events of diversified properties are presented in §3. Our statistical results on post-impulsive-phase accelerations are shown in §4. The more general relations between CMEs and flares are given in §5 followed by a summary and discussions in §6.

2. Observations and Data

In this study, we make use of CMEs observed during 1996–2006 by the the Large Angle and Spectrometric Coronagraph (LASCO) (Brueckner et al. 1995) on board the Solar and Heliospheric Observatory (SOHO). The two complementing LASCO coronagraphs, C2 and C3, have fields of view (FOVs) of $2.2\text{--}6.0 R_{\odot}$ and $4.0\text{--}30 R_{\odot}$, respectively. Flare data are from GOES satellites providing the full disk soft X-ray emission from the Sun in $1\text{--}8 \text{ \AA}$. The RHESSI (Reuven Ramaty High Energy Solar Spectroscopic Imager; Lin et al. 2002) and YOHKOH SXT (Soft X-ray Telescope) provide the hard X-ray light curves for some of the flares studied in this paper. However, the hard-X-ray flare data do not enter the statistical study in this paper.

From 1996–2006, there are in total about 11536 CMEs observed by LASCO according to the CDAW CME catalog, and 22686 flares seen by GOES based on the NOAA flare catalog. Because of the sheer number, we limit our study only to major flares; these are 1425 M-class and 120 X-class flares, and 1545 in total. In order to find out only those flares associated with CMEs (the so-called eruptive flares), an easy and quick approach is to use the so called time-window method, without resorting to inspecting images (Harrison 1995, Yashiro et al. 2005). The CME onset time is estimated through a backward extrapolation to the surface at $1.0 R_{\odot}$ from the height-time observations in coronagraph assuming a constant velocity. An association is assumed if a flare occurs within a certain time window centered at the estimated CME onset time, e.g., ± 60 minutes. We find that this simple time-window method can make successful association for most of events ($\sim 85\%$). However, there is a certain percentage of wrong association, which may not be acceptable for serious studies, e.g., the work presented in this paper and predicting CMEs from flare observations. The wrong association arises from the chance association, e.g., between a confined solar flare occurring on the front-side of the Sun and a CME occurring on the back-side of the Sun.

In this paper, we use a more strict method to associate flares and CMEs, by visually inspecting the movies observed by LASCO with the those by EIT (Extreme-ultraviolet Imaging Telescope, also on board SOHO, Delaboudinière et al. 1995) one by one, although it is tedious and time consuming. In addition to be used to identify the location of flares through transient brightening in a small compact patch, EIT data are also commonly used to identify the source region of CMEs through the signature of large scale dimming and/or wave, which are often prominent for major eruptions. The CME is taken for being associated with flare if the temporal-spatial co-registration of transient flare brightening and the large scale dimming on EIT images occurs, which is the most reliable way to associate flares and CMEs.

Among the 1545 major solar flares recorded by NOAA, 1246 events have both EIT and LASCO observations; the other 299 flares occurred in a period of either EIT or LASCO data gap (or both). For these 1246 flares, we find that 706 events (56.6%) are associated with CMEs, while the other 540 flares (43.4%) are confined. These confined flares will not be used in this study. Further, we eliminate those events with less than 5 effective snapshot observations during the two-hour window of calculating the post-impulsive-phase acceleration (explained in the next paragraph). We also remove those events without effective C2 observations. In the end, we obtain 247 flare-CME pairs suitable for the study in this paper.

To determine the magnitude of the post-impulsive-phase acceleration, we calculate the average acceleration within the fixed time window of two hours beginning at the peak time of the associated flare. While the post-impulsive-phase refers to the CME evolution, we have adopted the flare peak time as the proxy of the starting time of this CME phase. The starting time is difficult to be determined directly from CME observations, due to the poor cadence and the lack of inner coronal observations of LASCO (except for a small number of events). Further, we believe that this proxy is a reasonable one because of the temporal coincidence between CME kinematic evolutions and flare flux variations (e.g., Zhang et al. 2001). The average acceleration is obtained through the second-order polynomial fitting of the observed height-time measurements in this window. We believe that such an average acceleration value is an effective representation of the post-impulsive-phase acceleration of the CME, whereas its validity may need to be further demonstrated using observations with higher cadence. As for the method of the fixed time window, we think that it is a good approach to characterize the relevant observation. In this approach, the beginning time of the post-impulsive-phase acceleration phase is uniform and well defined, that is the peak time of the associated flare. On the other hand, for this type of observational study of calculating an average property from a limited number of data points, one has to choose the

most appropriate window. We think that the selection of a two-hour window is reasonable; it is long enough to have sufficient number of data points to make a second-order polynomial fitting to the CME height-time measurement, while is short enough to differentiate the coronal effect on the dynamic evolution from the otherwise dominant solar wind effect on CME evolution in the later phase of the propagation in the LASCO FOV. Furthermore, we have checked the influence of the different time window on the data and find that there is always a weak correlation between the CME post-impulsive-phase acceleration and the associated-flare decay time. Therefore, similar results are obtained if a different time window is adopted.

Note that the average acceleration through the fixed time window carries much smaller error than the uncertainty inferred from any piece-wise fitting method. In general, the acceleration is much more difficult to calculate than the speed due to the nature of differentiation on discrete data points; the error bars in the acceleration values are significantly larger than those in the speed values (Zhang et al. 2006; Yashiro et al. 2004). For one specific data point, the acceleration error could be comparable to the inferred acceleration value. However, the error in the average acceleration based on the second-order polynomial fitting of at least five observed height-time measurements becomes significantly smaller.

3. Examples

Before we show the statistical properties of CME post-impulsive-phase acceleration and flare decay time, we present in detail four individual events, two of which are of positive acceleration and the other two are of negative acceleration. The overall properties of these four events are summarized in Table 1, including CME velocity, impulsive acceleration, post-impulsive-phase acceleration, acceleration error, flare rise time, decay time, location

and peak intensity.

3.1. CME Positive Post-Impulsive-Phase-Acceleration and Flare Long-Decay Time

3.1.1. 2001 September 24 Event

The CME on 2001 September 24 is associated with a GOES X2.6 class flare. Figure 1 shows the velocity-time plot of the CME (broken lines with symbols) along with the GOES X-ray time profiles (solid line). The CME onset time, estimated through linear extrapolation of the height-time measurement, was at 10:21 UT while the associated flare started at 09:32 UT; there is an 49 minute difference between the two onset times. We argue that, if inner corona observation were available, one would expect to find that the CME onset time coincide with the flare onset, probably within a few minutes. The time difference we find here is due to the usage of linear extrapolation assuming a constant speed in the inner corona, which is apparently an over simplification of the true evolution involving significant acceleration from almost zero speed to the final speed (e.g., Zhang et al. 2001). The heliographic location of the flare was S16 E23, which is consistent with the CME feature position angle of 142° . The feature position angle is defined as the most distinguishable feature used to measure the height. Here, we use the feature position angle instead of the center position angle because the CME is a halo CME when it appears in the FOV of LASCO/C3. The CME first appeared in the FOV of the C2 image at 10:30 UT at a height of $3.3 R_\odot$ from the disk center. As shown in Figure 1, the CME reached a velocity at about 2000 km s^{-1} at the peak time of the flare. What is important of this event is that it continued to accelerate during two hours after the peak time of the flare, from about 2000 to 2500 km s^{-1} ; during this period, the CME leading edge moved from about $3 R_\odot$ to $25 R_\odot$. The post-impulsive-phase acceleration during the fixed time window

is about 64 m s^{-2} , as determined by the second-order polynomial fitting of the height-time measurements. On the other hand, the inferred CME impulsive acceleration during the impulsive acceleration phase is about 455 m s^{-2} , using the flare rise time as a proxy of the time of CME impulsive acceleration (Zhang et al. 2006). Note that the uncertainty of the CME speed comes mainly from the uncertainty in height measurements, which are estimated to be about 8 pixels in the original images, or about 0.10 and $0.47 R_{\odot}$ for C2 and C3, respectively. In the same way, the uncertainty in height measurements also determined the acceleration uncertainty, which is $\pm 58 \text{ m s}^{-2}$ for this event. The same uncertainties are used for other events discussed in this paper. We note that the uncertainties may be even larger than such determined for CME events with less sharp leading edges. The flare peaked at 10:38 UT and ended at 11:09 UT with a decay time of 31 min; the ending time is defined by NOAA as the time of the half-maximum. The flare is apparently a long decay flare as seen from the temporal profile of the SXR emission in Figure 1. The decay phase lasts longer than the radiation cooling time scale (about 20 minutes), so there must be the continuing energy released to delay the radiation cooling time. We believe that the observed post-impulsive-phase acceleration of this CME is related with the continuing energy release following the impulsive energy release phase known for such a long-decay flare. Continuing driving force is needed, not only to overcome the aerodynamic dragging force of the background solar wind, but also to further accelerate the CME.

3.1.2. 2003 November 18 Event

The CME on 2003 November 18 is another example of events showing positive post-impulsive-phase acceleration. It is a CME associated with a GOES M4.5 class flare (Figure 2). The estimated CME onset time from linear extrapolation is 9:43 UT and the associated flare started at 9:23 UT. The heliographic coordinate of the flare was S14E89

and the feature position angle of the CME that was about 87° . The CME first appeared in the FOV of C2 at 9:50 UT at a height of $2.9 R_\odot$. As from Figure 2, the CME was continuously accelerated from about 1300 to 1900 km s^{-1} during two hours after the peak time of the flare. The post-impulsive-phase acceleration and its error are about 40 m s^{-2} and $\pm 36 \text{ m s}^{-2}$, respectively. On the other hand, the estimated impulsive acceleration during the impulsive acceleration phase is about 632 m s^{-2} . The flare peaked at 10:11 UT and ended at 11:01 UT with a decay time of 50 min, which implies a long decay behavior of the flare.

3.2. CME Negative Post-Impulsive-Phase-Acceleration and Flare Short-Decay Time

3.2.1. 2004 October 20 Event

Different from the previous two events, we show examples of CMEs with negative post-impulsive-phase acceleration, or deceleration following the impulsive acceleration phase. In Figure 3, we shown a CME that occurred on 2004 October 20 and was associated with a GOES M2.6 class flare. The CME onset time was 10:32 UT and the associated flare started at 10:43 UT. The position of the flare was N11 E68. The center position angle and width of the CME were 68° and 123° , respectively. It is evident that the CME was decelerated from about 1100 to 700 km s^{-1} during two hours after the peak time of the flare, as seen from the velocity profile of the event in Figure 3. The post-impulsive-phase acceleration and its error of the CME are about -71 m s^{-2} and $\pm 37 \text{ m s}^{-2}$ in the fixed time window, respectively. The flare peaked at 10:51 UT and ended at 10:56 UT with a decay time of only 5 min. This event indicates that a CME, when is associated with a short decay flare, lacks the continuing driving force and therefore suffer significant deceleration after the impulsive acceleration phase.

3.2.2. 2005 August 25 Event

The following is another example of CMEs of negative post-impulsive-phase acceleration. The fast CME was observed on 2005 August 25 and was associated with a GOES M6.4 class flare. The CME onset time was 4:16 UT and the associated flare started at 4:31 UT. N09 E80 was the site of the flare. The center position angle and width of the CME were 75° and 146° , respectively. The LE of the CME was very sharp and can be easily identified from the running-difference images. It had a velocity of about 2000 km s^{-1} when appeared in the FOV of C2. The velocity profile of this CME in Figure 4 shows that the CME was decelerated from about 2000 to 1400 km s^{-1} in about 2 hours. The post-impulsive-phase acceleration and its error of the CME are -129 m s^{-2} and $\pm 41 \text{ m s}^{-2}$, respectively. The flare peaked at 04:40 UT and ended at 04:45 UT. The decay phase of the flare lasted only 5 min in the SXR temporal profile.

4. Statistics on CME Post-impulsive-phase Acceleration and Flare Decay Time

Having presented examples of two distinct types of events, we now look into the statistical behavior. Figure 5 shows the distribution of the post-impulsive-phase acceleration of CMEs vs. the decay time of the associated flares for all the 247 events studied. As shown by the linear fitting line in Figure 5, there is a general trend that the longer the decay time of flares, the larger the post-impulsive-phase acceleration of CMEs. On the other hand, the correlation between CME post-impulsive-phase acceleration and flare decay time is rather poor. There is an apparent-wide scattering of the parameters in both dimensions. The acceleration varies in a wide range from -150 m s^{-2} to 180 m s^{-2} and tends to change from negative to positive value with the decay time of the associated flares increasing. The fraction of CME events with positive post-impulsive-phase acceleration apparently

increases as the decay time of the associated flare increases. The mean post-impulsive-phase acceleration of all events is negative at about -11.9 m s^{-2} , as indicated by the solid thin line in the Figure.

For the sake of clarity of discussion, we divide the events into three different groups, as enclosed by the three rectangular boxes in the Figure: positive-post-impulsive-acceleration CMEs with long-decay flares (acceleration-long, or A-L), negative-post-impulsive-acceleration CMEs with short-decay flares (deceleration-short, or D-S), and positive-post-impulsive-acceleration CMEs with short-decay flares (acceleration-short, or A-S). Apparently, there is a lack of CME events of deceleration with long-decay flares; those CMEs associated with long decay flares tend to have positive post-impulsive-phase acceleration, even though they have reached a high speed at the end of the impulsive acceleration. It is commonly believed that there is a continuing energy release during the decay phase of long duration flares. Therefore, this statistical result implies that the continuing energy release also related with the continuing acceleration of CMEs in the outer corona.

Nevertheless, for events with short flare decay times, the post-impulsive-phase acceleration could be either positive or negative. One would expect that the post-impulsive-phase acceleration tends to be negative for events associated with short-decay flares, since there is no further energy available for accelerating CMEs following the main energy release phase. However, we believe that the influence of solar wind dragging force makes the matter complex. It is known that the solar wind dragging force accelerates slow CMEs and decelerate fast CMEs; the magnitude depends on the relative velocity between CME and solar wind, the drag coefficient and the CME cross section size (Cargill 2004). Indeed, we identify that many positive-acceleration-short-decay events (A-S) are slow CMEs. These slow CMEs also tend to be narrow and weak. Because of the slowness of these events, the

positive acceleration is likely to be caused by the dragging force of the background solar wind, instead of the continuing energy release that only occurs in A-L type events. Further, slow and narrow CME events often appear weak in brightness and thus fuzzy in morphology as seen in coronagraph images. As a consequence, it is usually hard to trace a consistent features such as leading edges (LE) for these event, leading to large error in the height-time measurements and thus larger error in the derived velocity.

In Figure 6, we show a similar scattering plot as in Figure 5 but use only events with fast CME speed ($>800 \text{ km s}^{-1}$) and wide CME angular width ($>60^\circ$). The general trend between CME post-impulsive-phase acceleration and flare decay time becomes more distinct than that in Figure 5. In essence, we want to argue that, for major fast and wide CMEs, the CMEs associated with long decay-time flares tend to be further accelerated in the outer corona, overcoming the slowing-down effect of solar wind dragging on fast CMEs. The CMEs associated with short decay-time flares tend to be decelerated in the outer corona, but may gain positive acceleration due to the solar wind dragging if the initial speed is slow.

5. General Statistical Relations Between CME and Flare Properties

In this section, we describe the more general relations between CMEs and flares from a statistical point of view. In Figure 7, we show the scattering plots between CME velocity and various flare parameters, including rise time, total duration, peak flux and total flux (or fluence). We find that the velocities of CMEs show almost no correlation or weak at best with the rise times or the total durations of the associated flares. However, there is a certain positive correlation between CME velocity and flare peak flux. This correlation has been noted before (Moon et al. 2002, 2003). The linear-fitting formula between CME velocity V (km s^{-1}) and flare peak flux F ($\text{Watt m}^2 \text{ s}^{-1}$) can be expressed as $V = 474.0 \log F + 2922.2$.

It is interesting that the best correlation is found between CME velocity and total flare flux or fluence; the total flux here is simply calculated through the product of the peak flux and the total duration of flares. The linear correlation coefficient is 0.54, which is better than that of any other flare parameters. The linear-fitting formula between CME velocity and flare fluence can be expressed as $V = 422.4 \log(F \cdot T) + 1321.6$, where F is the peak flux and T is the total duration in second. The total soft X-ray flux of a flare is believed to be a good measure of the total energy released during the flare. Therefore, this correlation result may be a manifestation that the final CME velocity is proportional to the total energy released in the corona. During the eruption process, part of the released coronal energy goes to CME bulk kinetic energy in the global scale, while the other part goes to flare plasma heating and particle acceleration in the microscopic scale. Magnetic reconnection is a likely physical process that produces both CME and flare energies, and also makes the amounts of the two energies comparable.

Figure 8 shows the relationship between the velocity and the angular width of CMEs. Apparently, there is a positive correlation; the correlation coefficient is 0.52 for all 247 CMEs and a much improved coefficient of 0.62 for 111 limb CMEs (heliographic longitude larger than 60°). It is not surprising that the limb CMEs show better correlation, since they are less subject to the project effect that artificially enlarges the apparent angular width. The linear-fitting formula for the limb CMEs is $V = 2.8W + 429.1$, where W is the apparent CME angular width in units of degree. The correlation coefficient obtained here is larger than that obtained for a larger sample of events by Yashiro et al. (2004)

Finally, we show the histogram distribution of the CME/flare parameters used in this study (Figure 9). Their overall statistical properties, including minimum value, maximum value, average value, medium value, mode (or the value at maximum distribution) and standard deviation are summarized in Table 2. The mean velocity of 747 km s^{-1} , for the

247 major events studied in this paper, is larger than the value of 684 km s^{-1} obtained by Moon et al. (2002). The mean impulsive acceleration of these CMEs is 939 m s^{-2} , whereas the post-impulsive-phase accelerations are limited to a small range centered near zero and the mean post-impulsive-phase acceleration is -11.9 m s^{-2} , being almost consistent with the results of Zhang et al. (2006).

6. Summary and Discussions

We have studied the statistical kinematic properties of major-flare-associated CME events occurred between 1996-2006, with a focus on the post-impulsive-phase acceleration. It has been well known that a typical flare-associated CME usually has a strong and impulsive acceleration in the inner corona, and the impulsive acceleration coincides well with the main energy release of the associated flare (Zhang et al. 2001; Gallagher et al. 2003; Vršnak et al. 2004; Temmer et al. 2008). In this paper, we further find that the post-impulsive-phase acceleration of CMEs may be also physically related with the continuing energy release. In particular, CMEs tend to have positive post-impulsive-phase acceleration if the associated flares have a long decay phase; this kind of flares is often called LDE (long duration event). When flare decay times are short, accompanying CMEs may have mixed response, possibly with positive or negative post-impulsive-phase acceleration from event to event.

We argue that the positive post-impulsive-phase acceleration of LDE events is driven by the continuing magnetic reconnection occurring during the flare decay phase. It is widely accepted that the main energy release phase of a solar flare is driven by magnetic reconnection in the inner corona. When a flare has a long decay phase, continuing magnetic reconnection is also needed to explain the lasting thermal emission. Without the continuing energy release, the typical thermal energy decay time, which is controlled by the radiation

cooling and also the thermal conduction to the cooler chromosphere, is only about 20 minutes (Forbes et al. 1989; Isobe et al. 2002). The idea of continuing reconnection has also been supported by observations of long-lasting post-flare loops (Schmieder et al. 1995, 1996; Czaykowska et al. 1999; Sheeley et al. 2004; Kołomanáski 2007). The observed rising motion of post-flare loops, as well as the observed separation motion of flare ribbons, are well explained by the reconnection model that these observed motions are driven by systematic rising of the reconnection point in the corona. The observed down-flows above post-flare arcades in the long-duration flares also support the idea of continuing reconnection (Mckenzie 2000; Sheeley et al. 2004). Similar connection between ribbon separation motion and coronal magnetic reconnection also occur in the main energy release phase (Qiu et al. 2004, 2005). Nevertheless, there must be certain differences between the reconnection during the main energy release phase and that during the decay phase. Isobe et al. (2002) found that in the decay phase the reconnection rate, and also the energy release rate, was about one-tenth of that in the rise phase. Therefore, it is reasonable to argue that the impulsive CME acceleration is driven by the fast reconnection in the impulsive phase, while the post-impulsive-phase CME acceleration is caused by the slow reconnection after the impulsive phase.

Chen et al. (2000, 2003, 2006) devised an analytic flux rope model to explain CME’s main and residual accelerations. It seems that the residual acceleration in the context of Chen’s model is similar to the post-impulsive-phase acceleration discussed in this paper, especially in terms of their magnitude and timing relative to that of the main phase. They showed that the main acceleration is attained before the CME reaches a critical height (below 2–3 R_{\odot}), and is then followed by the residual acceleration. The main acceleration phase is dominated by the Lorentz self-force through the injection of the poloidal magnetic flux of the flux rope, while the residual acceleration is dominated by the solar wind aerodynamic dragging force (Chen et al. 2003). On the other hand, in the

scenario of magnetic reconnection models, the CME impulsive acceleration is driven by the fast reconnection. It is kind of runaway tether-cutting reconnection not only cutting off the field lines tied to the photosphere and lessening the restraint of the overlying field but also rapidly increasing the magnetic pressure below the flux rope due to an added poloidal flux (Moore et al. 2001; Zhang et al. 2006). When the runaway tether-cutting reconnection ceases, the impulsive acceleration stops. However, for the CME associated with a long decay flare, even though it has departed from the Sun and may have already moved to as far as several solar radii from the Sun, the reconnection process may continue; it is most evident in the formation of the post-eruption loop arcades. The continued reconnection may further drives the CME and thus produce the positive post-impulsive-phase acceleration of the CME. Note that, the difference between the impulsive acceleration and the post-impulsive-phase acceleration may be mainly their different reconnection rates. A question may arise with respect to how to connect the positive post-impulsive-phase acceleration in the outer corona with the reconnection site close to the surface of the Sun. A possible explanation is that the reconnection magnetic fields are overlying fields surrounding the CME leading edge in the outer corona but are stretched up open in the low corona. Therefore, the post-impulsive-phase acceleration of the CME in the outer corona and the energy release of the associated flare in the decay phase are different manifestations of the slow magnetic reconnection following the fast magnetic reconnection.

On the other hand, when the associated flare is of short duration, one does not expect continuing reconnection and thus continuing acceleration of the CME. Indeed, about half CMEs with short-duration flares have suffered deceleration in the outer corona, or negative post-impulsive-phase acceleration. Nevertheless, many CMEs associated with short-duration flares have also showed positive post-impulsive-phase acceleration. Detailed investigation shows that these CMEs tend to be slow, narrow and weak. It is likely that the positive acceleration is caused by the solar wind dragging force, which acts as a positive

driving force when the embedded object is slower. The full dynamic evolution of a CME shall involve not only the various Lorentz forces caused by current-carrying magnetic fields, but also the solar wind dragging force. For those fast CME events associated with long decay flares, even though the solar wind dragging force is a decelerator of CMEs, the positive Lorentz force caused by continuing magnetic reconnection is able to overcome the dragging and further accelerating the already-fast CMEs. This scenario helps explain why certain number of CMEs are extremely fast.

We thank the anonymous referee for many valuable suggestions and comments that helped to improve the paper significantly. We are grateful to P. F. Chen and M. Jin for discussions and help in data analysis. J. Z. thanks Seji Yashiro for providing the text file of the CDAW CME catalog and his version of CME-flare list. J. Z. and W. P. acknowledge the support from NSF grant ATM-0748003 and NASA grant NNG05GG19G. X. C. and M. D. D. are supported by NSFC under grants 10673004, 10828306, and 10933003 and by NKBRFSF under grant 2006CB806302. We acknowledge the use of the CDAW CME catalog, which is generated and maintained at the CDAW Data Center by NASA and The Catholic University of America in cooperation with the Naval Research Laboratory. SOHO is a project of international cooperation between ESA and NASA. Yohkoh is a project of international cooperation between Japan, US and UK.

REFERENCES

- Andrews, M. D., & Howard, R. A. 2001, *Space Sci. Rev.*, 95, 147
- Andrews, M. D. 2003, *Sol. Phys.*, 218, 261
- Brueckner, G. E., et al. 1995, *Sol. Phys.*, 162, 357
- Burkepile, J. T., Hundhausen, A. J., Stanger, A. L., St.Cyr, O. C., & Seiden, J. A. 2004, *J. Geophys. Res.*, 109, A03103
- Delaboudinière, J. P., et al. 1995, *Sol. Phys.*, 162, 291
- Cargill, P. J. 2004, *Sol. Phys.*, 221, 135
- Chen, J., et al. 2000, *ApJ*, 533, 481
- Chen, J. & Krall, J. 2003, *J. Geophys. Res.*, 108(ALL), 1410(PaperI)
- Chen, J., Marqué, C., Vourlidas, A., Krall, J., & Schuck, P. W. 2006, *ApJ*, 649, 452
- Czaykowska, A., Alexander, D., & De Pontieu, B. 1999, *ApJ*, 521, L75
- Gallagher, P. T., Lawrence, G. R., & Dennis, B. R. 2003, *ApJ*, 588, L53
- Gosling, J. T. 1993, *J. Geophys. Res.*, 98, 18937
- Harrison, R. A. 1995, *A&A*, 304, 585
- Hundhausen, A. J., 1999, in *The Many Faces of the Sun*, ed. K. Strong, et al. (New York: Springer), 143
- Isobe, H., et al. 2002, *ApJ*, 566, 528
- Kahler, S. M. 1992, *ARA&A*, 30, 113

- Koľomanáski, S. 2007, *A&A*, 465, 1035
- Lin, J., & Forbes, T. G., 2000, *J. Geophys. Res.*, 105, 2375
- Lin, R. P., et al. 2002, *Sol. Phys.*, 210, 3
- MacQueen, R. M., & Fisher, R. R. 1983, *Sol. Phys.*, 89, 89
- Marićić, D. et al. 2007, *Sol. Phys.*, 241, 99
- Mckenzie, D. E. 2000, *Sol. Phys.*, 195, 381
- Moon, Y.-J., Cho, K. S., Wang, H., Park, Y. D., Gopalswamy, N., Yang, G., & Yashiro, S. 2002, *ApJ*, 581, 694
- Moon, Y.-J., Cho, K. S., Wang, H., Park, Y. D., & Cheng, C. Z. 2003, *J. Korean Astron. Soc.* 36, 61
- Moore, R. L., Sterling, A. C., Hudson, H. S., & Lemen, J. R. 2001, *ApJ*, 552, 833
- Neupert, W. M., Thompson, B. J., Gurman, J. B., & Plunkett, S. P. 2001, *J. Geophys. Res.*, 106, A11, 25215
- Forbes, T.G., Malherbe, J. M., & Priest, E. R. 1989, *Sol. Phys.*, 120, 285
- Priest, E. R., & Forbes, T.G. 2002, *A&A Rev.*, 10, 313
- Qiu, J., Wang, H., Cheng, C. Z., & Gary, D. E. 2004, *ApJ*, 604 900
- Qiu, J., & Yurchyshyn, V. B. 2005, *ApJ*, 634 L121
- Schmieder, B., Heinzl, P., Wiik, J. E., Lemen, J. R., Anwar, B., Kotrc, P. & Hiei, E. 1995, *Sol. Phys.*, 156, 337
- Schmieder, B., Heinzl, P., van Driel-Geztelyi, L., & Lemen, J. R. 1996, *Sol. Phys.*, 165, 303

- Shanmugaraju, A., Moon, Y.-J., Dryer, M., & Umapathy, S. 2003 *Sol. Phys.*, 215, 185
- Sheeley, N. R., Warren, H. P., & Wang, Y. -M. 2004, *ApJ*, 616, 1224
- St. Cyr, O. C., Burkepile, J. T., Hundhausen, A. J., & Lecinski, A. R. 1999, *J. Geophys. Res.*, 104, 12493
- Temmer, M., Veronig, A. M., Vršnak, B., Rybák, J., Gömöry, P., Stoiser, S., & Maričić, D. 2008, *ApJ*, 673, L95
- Vršnak, B., et al. 2004, *Sol. Phys.*, 225, 355
- Vršnak, B., & Skender, M. 2005, *Sol. Phys.*, 226, 97
- Webb, D. F., Forbes, T. G., & Aurass, H. et al. 1994, *Sol. Phys.*, 153, 73
- Yashiro, S., Gopalswamy, N., Michalek, G., St. Cyr, O. C., Plunkett, S. P., Rich, N. B., & Howard, R. A. 2004, *J. Geophys. Res.*, 109, 07105
- Yashiro, S., Gopalswamy, N., Akiyama, S., Michalek, G., & Howard, R. A. 2005, *J. Geophys. Res.*, 110 ,A12S05
- Yashiro, S., Akiyama, S., Gopalswamy, N., & Howard, R. A. 2006, *ApJ*, 650, L143
- Zhang, J., Dere, K. P., Howard, R. A., Kundu, M. R., & White, S. M. 2001, *ApJ*, 559, 452
- Zhang, J., Dere, K. P., Howard, R. A. & Vourlidas, A. 2004, *ApJ*, 604, 420
- Zhang, J., & Dere, K. P. 2006, *ApJ*, 649, 1100
- Zhang, M., & Golub, L. 2003, *ApJ*, 595, 1251

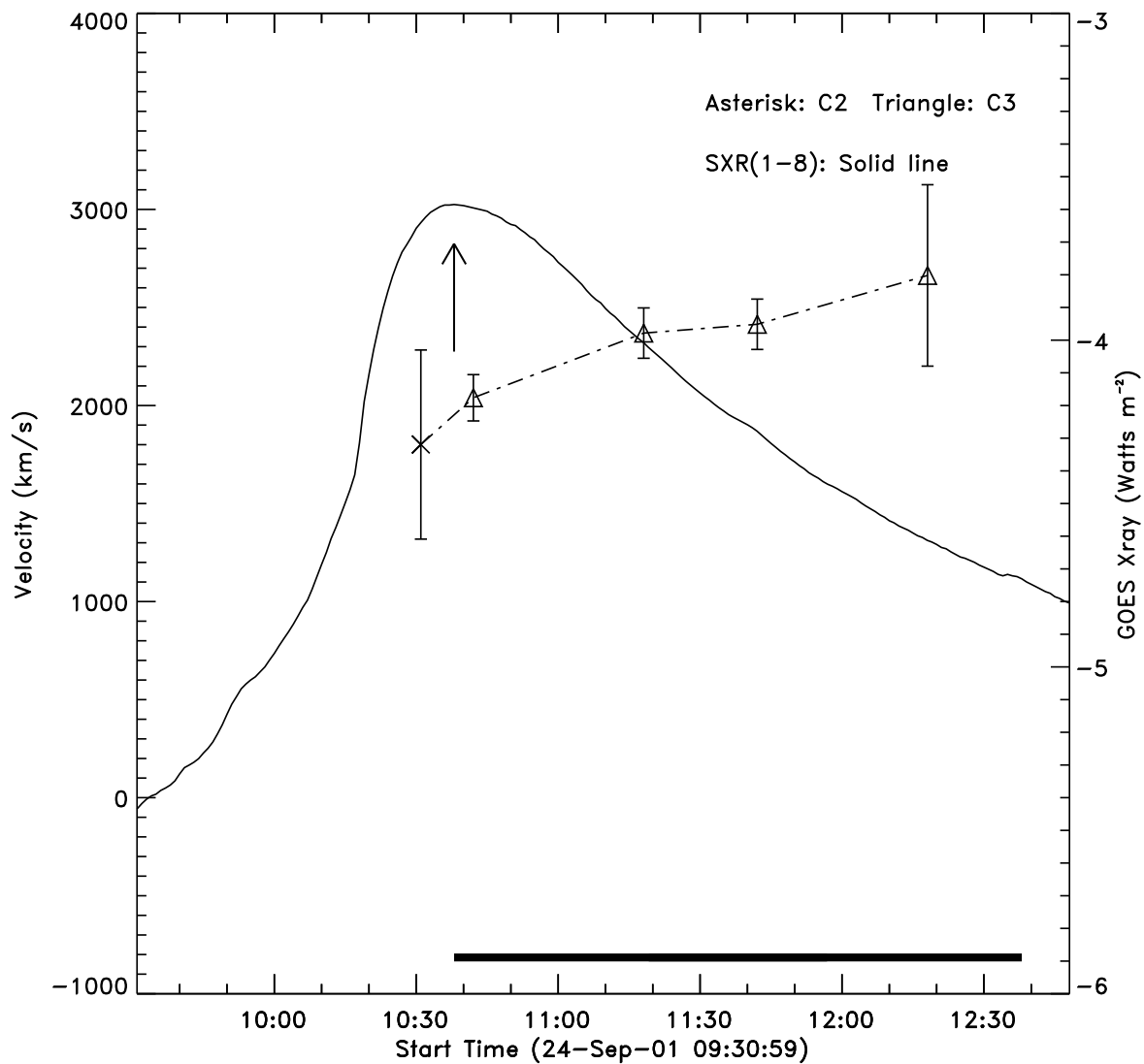


Fig. 1.— The velocity evolution of 2001 September 24 CME (broken line with symbols) and the temporal profile of the GOES SXR flux of the associated flare (solid line); the arrow denotes the peak time of the flare and the onset of the post-impulsive-phase acceleration of the CME. The horizontal bar indicates the two-hour window used to calculate the post-impulsive-phase acceleration. The CME has a positive post-impulsive-phase acceleration and the flare is of long-decaying.

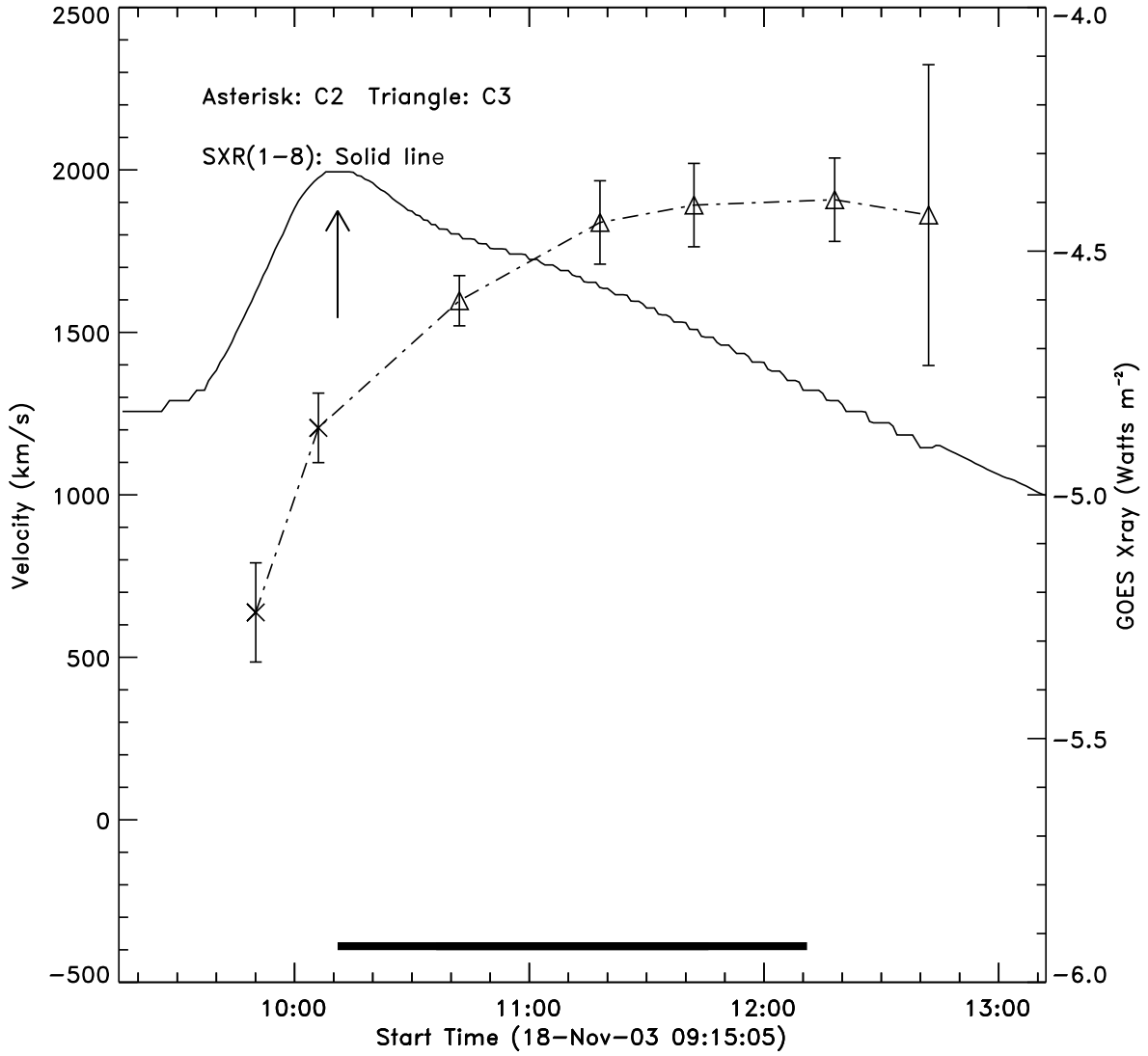


Fig. 2.— The velocity evolution of 2003 November 18 CME (broken line with symbols) and the temporal profile of the GOES SXR flux of the associated flare (solid line). The CME has a positive post-impulsive-phase acceleration and the flare is of long-decaying.

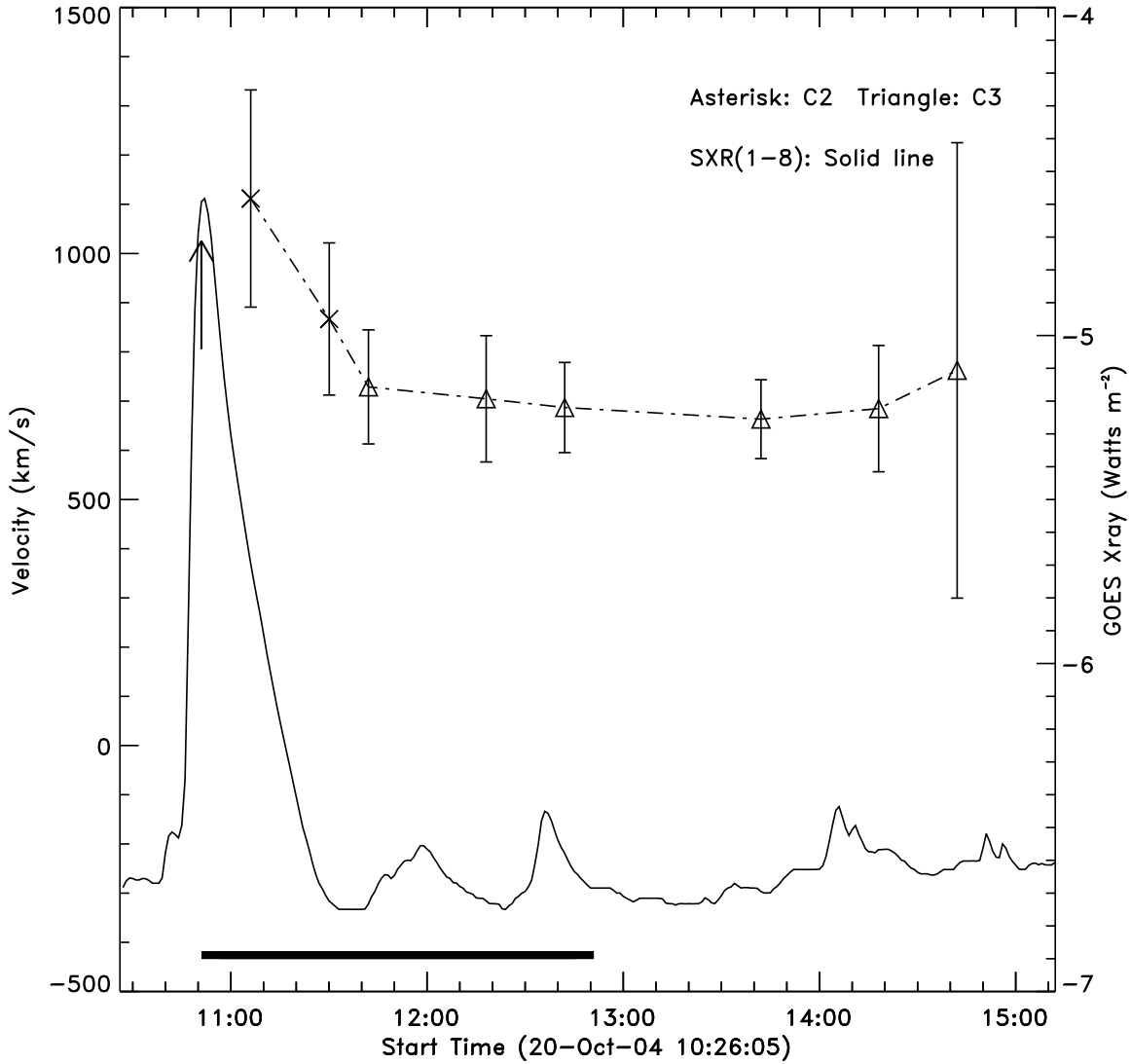


Fig. 3.— The velocity evolution of 2004 October 20 CME (broken line with symbols) and the temporal profile of the GOES SXR flux of the associated flare (solid line). The CME has a negative post-impulsive-phase acceleration and the flare is of short-decaying.

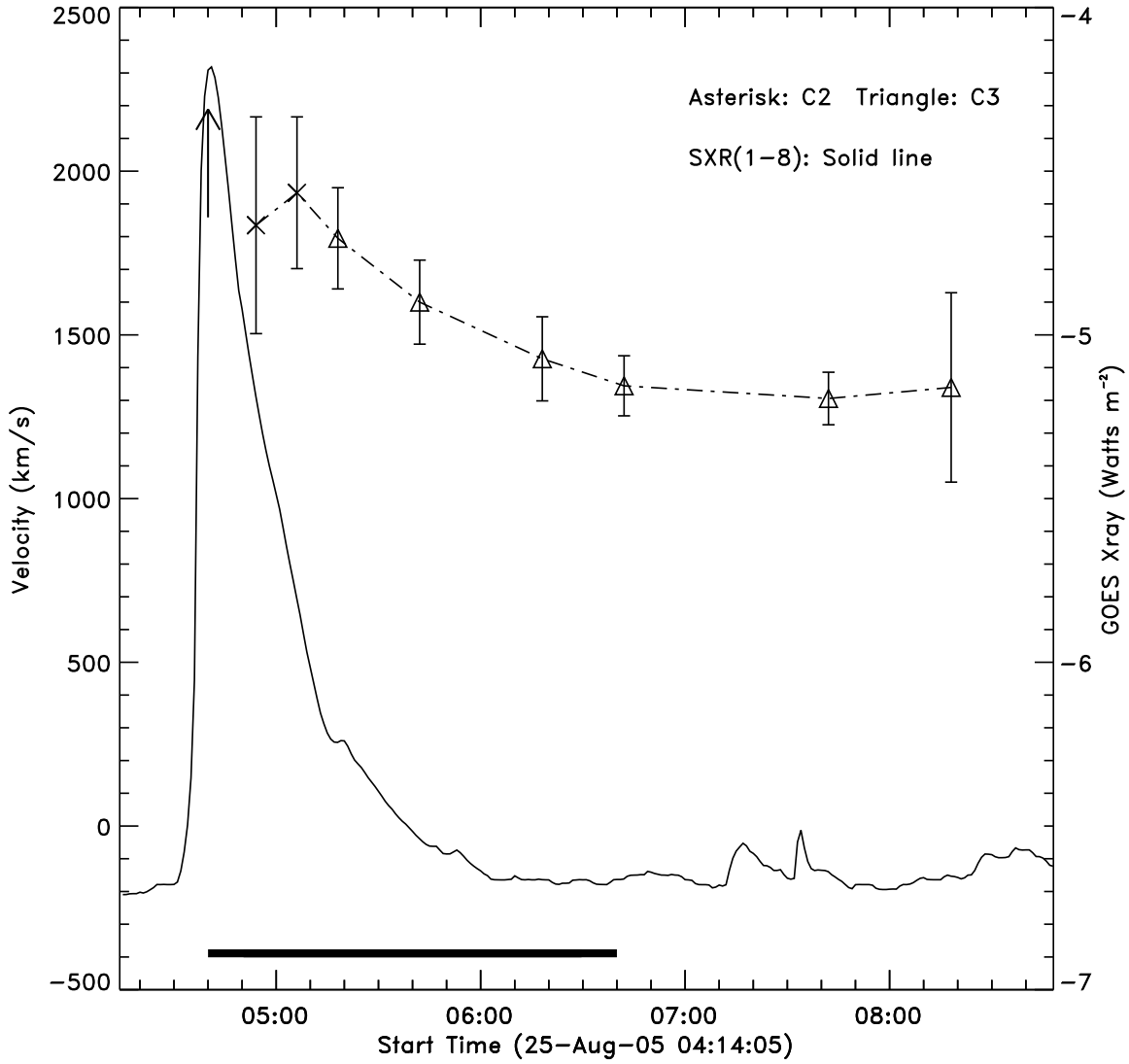


Fig. 4.— The velocity evolution of 2005 August 25 CME (broken line with symbols) and the temporal profile of the GOES SXR flux of the associated flare (solid line). The CME has a negative post-impulsive-phase acceleration and the flare is of short-decaying.

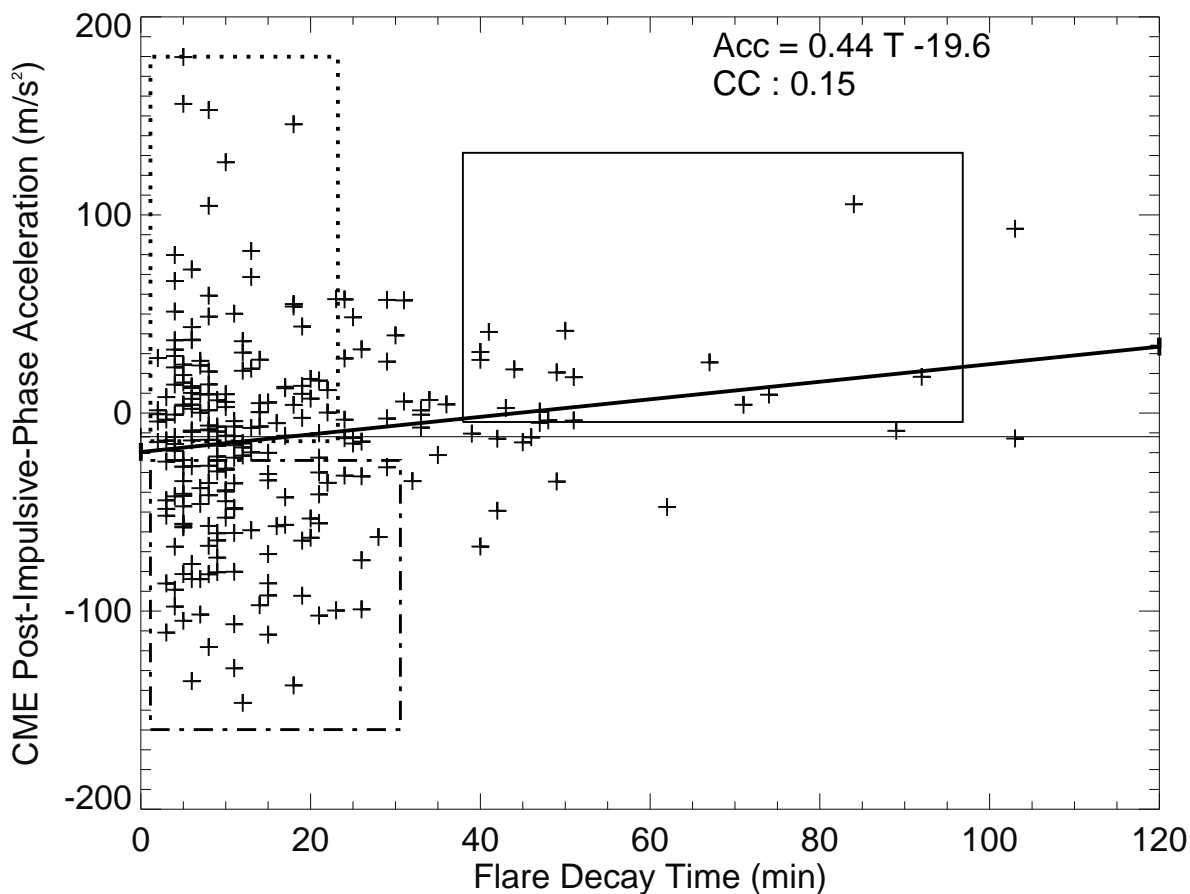


Fig. 5.— Scattering plot of CME post-impulsive-phase acceleration vs. flare decay time for all the 247 CME-flare events studied in this paper. The solid bold line denotes the linear fit to the points. The solid thin line indicates the average post-impulsive-phase acceleration of all events. The three rectangles group events into different types: acceleration CMEs with long-decay flares (A-L) (solid), deceleration CMEs with short-decay flares (D-S) (dash-dotted), and acceleration CMEs with short-decay flares (A-S).

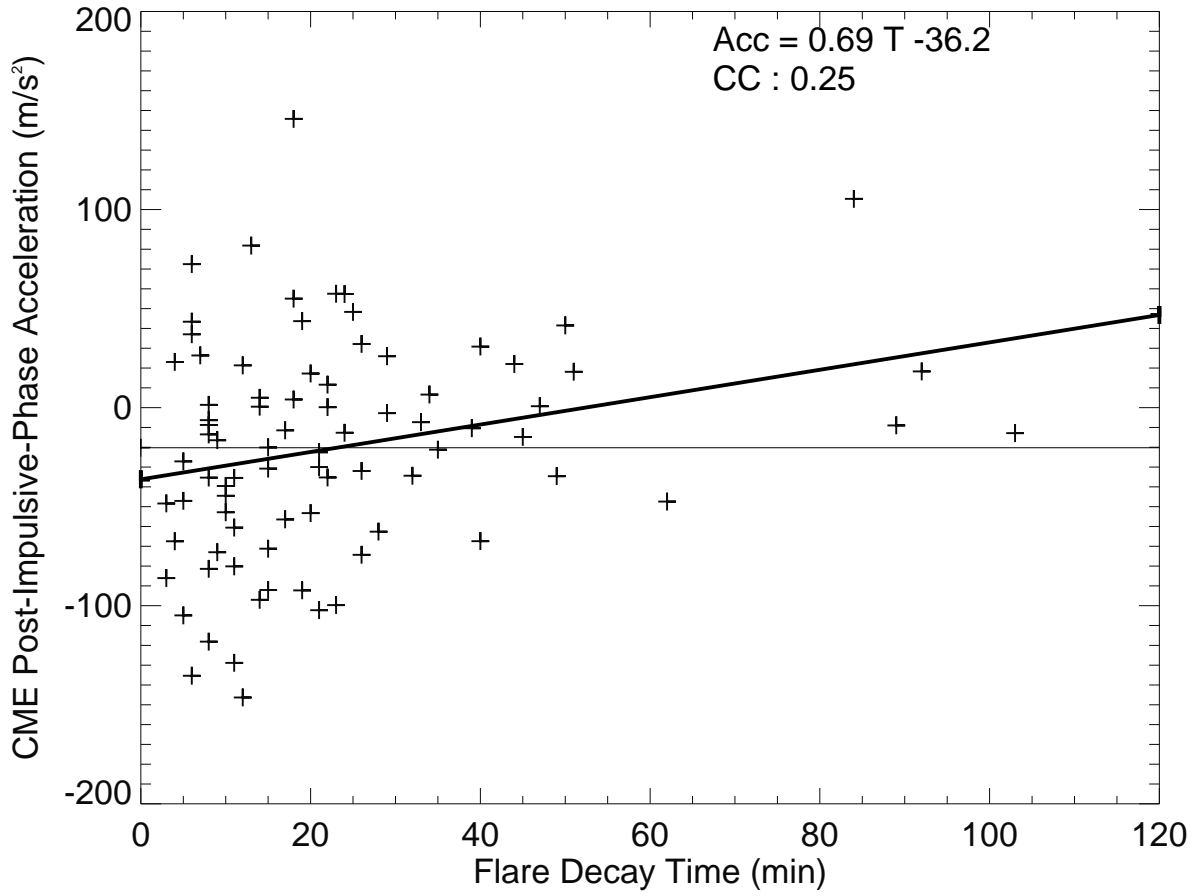


Fig. 6.— Scattering plot of CME post-impulsive-phase acceleration vs. flare decay time for 82 fast and wide CMEs (velocity $\geq 800 \text{ km s}^{-1}$ and width $\geq 60^\circ$). The solid bold line denotes the linear fit to the points. The solid thin line indicates the average post-impulsive-phase acceleration of these events.

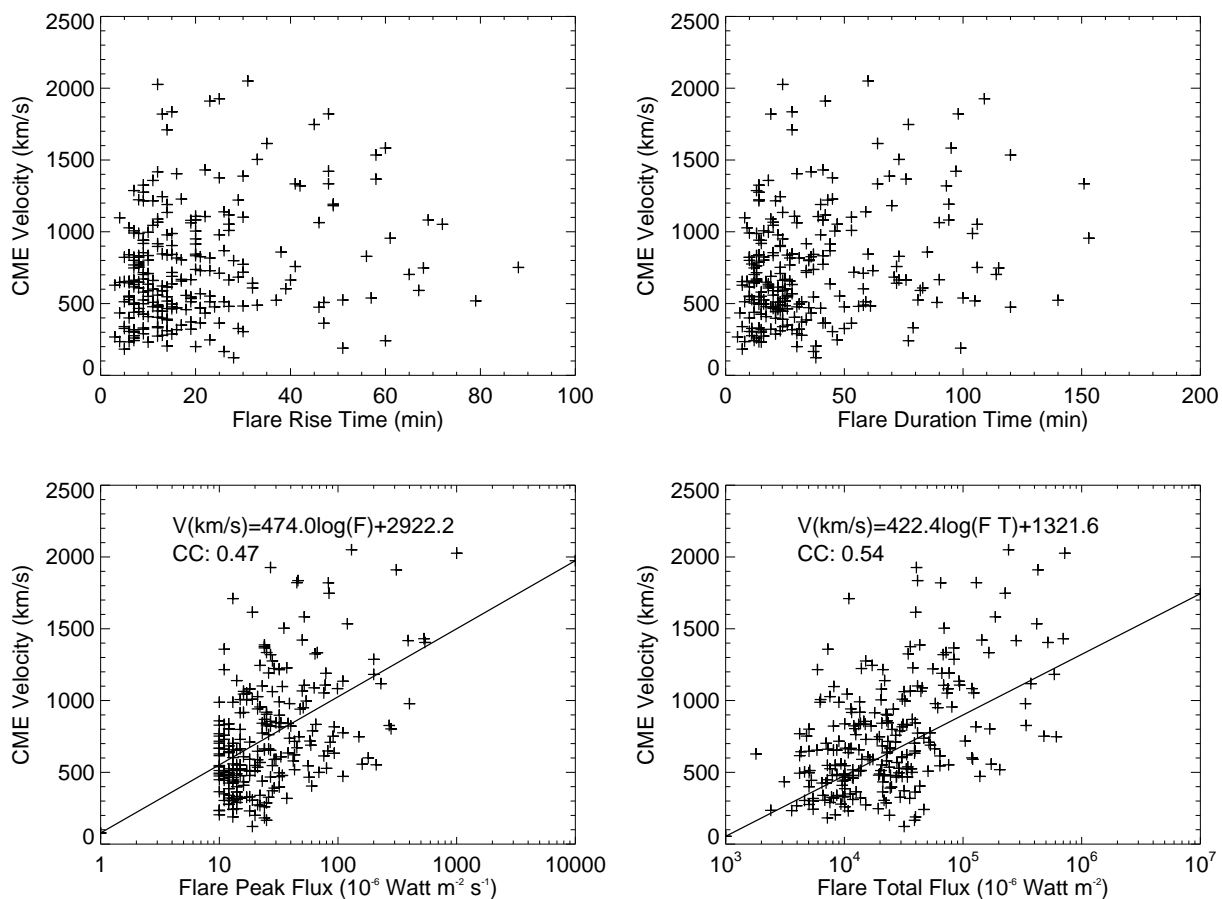


Fig. 7.— Scattering plots of CME velocity versus various flare properties: versus flare rise time (top-left panel), versus flare total duration (top-right panel), versus flare peak flux (or magnitude) (bottom-left panel) and versus flare total flux (or fluence) (bottom-right panel). The linear correlation fit is carried out in the two bottom panels. Apparently, the CME velocity-flare total flux has the best correlation with a coefficient of 0.54.

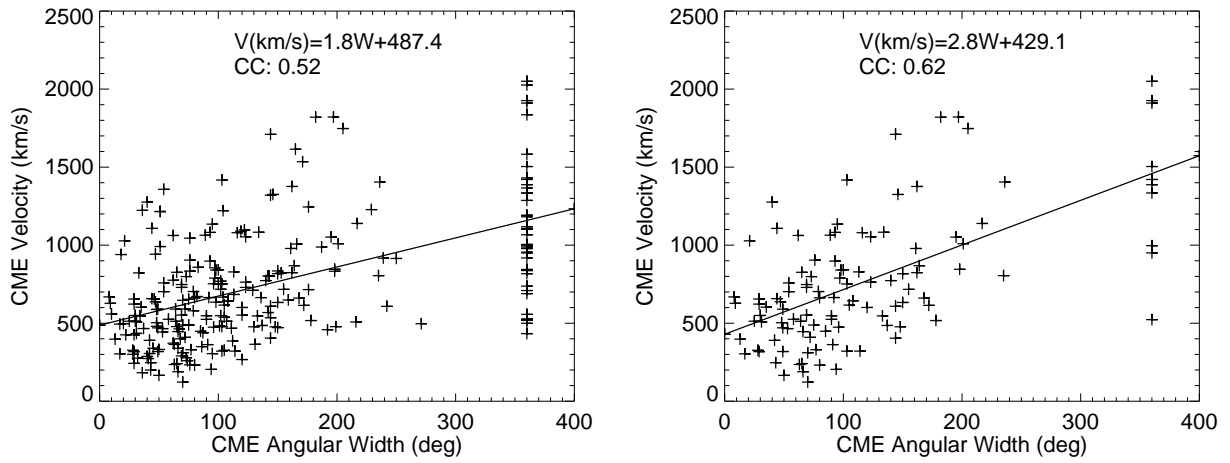


Fig. 8.— Scattering plots of CME velocity versus CME angular width for all the 247 events (left panel) and 111 limb events (right panel). Solid lines are linear-correlation fit. CC denotes the correlation coefficient.

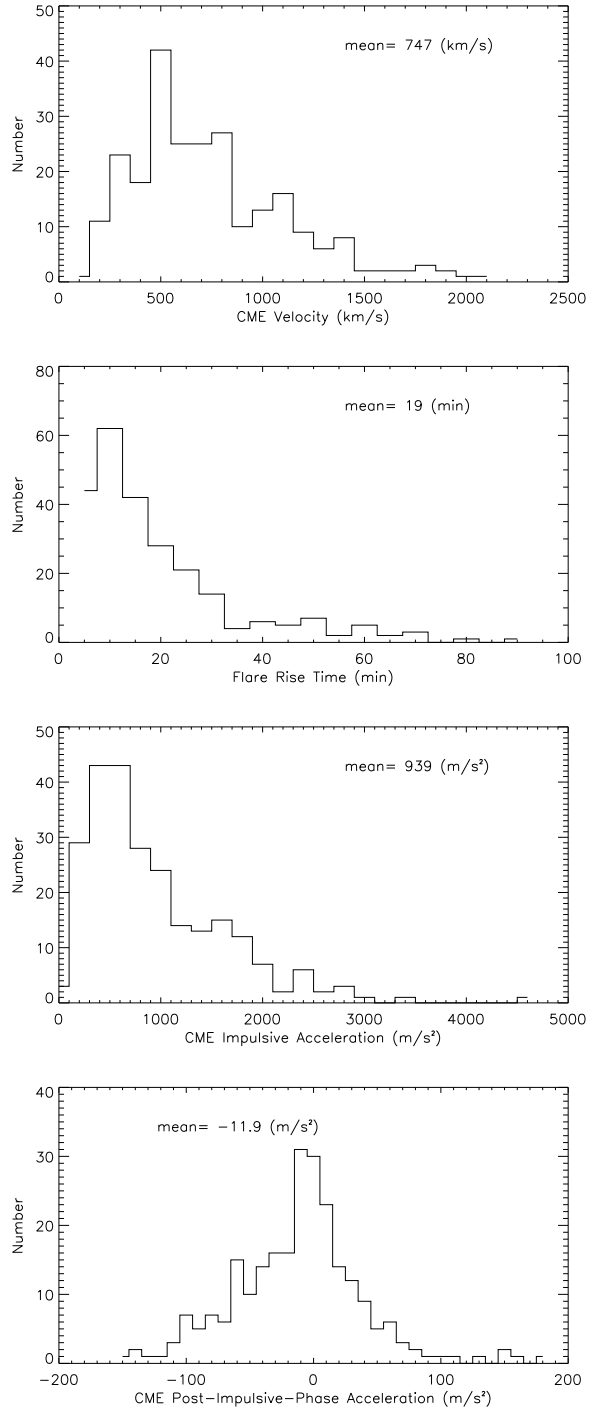


Fig. 9.— Histograms of CME and flare properties.

Table 1: Properties of Four Typical CME-flare Events.

| Event | Property | Velocity (km s ⁻¹) | Im. Acc ^a (km s ⁻²) | Post. Acc ^b (km s ⁻²) | (errors) | Rise (min) | Decay (min) | Location (deg) | Magnitude |
|-------------|----------|-----------------------------------|---|---|----------|---------------|----------------|-------------------|-----------|
| 2001 Sep 24 | A-L | 2402 | 455 | 64 (±58) | | 66 | 31 | S16E23 | X2.6 |
| 2003 Nov 18 | A-L | 1821 | 632 | 40 (±36) | | 48 | 50 | S14E89 | M4.5 |
| 2004 Oct 20 | D-S | 763 | 1589 | -71 (±37) | | 8 | 5 | N11E68 | M2.6 |
| 2005 Aug 25 | D-S | 1327 | 2453 | -129 (±41) | | 9 | 5 | N09E80 | M6.4 |

^aMagnitude of impulsive acceleration

^bMagnitude of post-impulsive-phase acceleration

Table 2: Statistical Values of CME/flare Properties.

| Parameters | Min | Max | Mean | Med | Mode | Sdev |
|---|--------|--------|-------|-------|-------|-------|
| Velocity (km s ⁻¹) | 123 | 2050 | 747 | 657 | 427 | 391 |
| Rise time (min) | 3 | 88 | 19 | 14 | 12 | 15 |
| Im. Acc ^a (m s ⁻²) | 61.8 | 4574.1 | 939.3 | 723.9 | 536.8 | 693.5 |
| Post. Acc ^b (m s ⁻²) | -146.3 | 179.7 | -11.9 | -9.4 | -9.0 | 51.0 |

^aMagnitude of impulsive acceleration

^bMagnitude of post-impulsive-phase acceleration